Charge and spin quantum fluctuations in the doped strongly coupled Hubbard model on the honeycomb lattice

F. G. Ribeiro[1,2] and M. D. Coutinho-Filho[1]

[1]*Laboratório de Física Teórica e Computacional, Departamento de Física, Universidade Federal de Pernambuco, Recife 50670-901, PE, Brazil*

[2]*Laboratório de Física, Núcleo de Tecnologia, Centro Acadêmico do Agreste, Universidade Federal de Pernambuco, Caruaru 55002-970, PE, Brazil*

(Received 9 April 2015; revised manuscript received 11 June 2015; published 6 July 2015; corrected 14 September 2015)

Field-theoretic methods are used to investigate the large-U Hubbard model on the honeycomb lattice at half-filling and in the hole-doped regime. Within the framework of a functional-integral approach, we obtain the Lagrangian density associated with the charge and spin degrees of freedom. The Hamiltonian related to the charge degrees of freedom is exactly diagonalized. In the strong-coupling regime, we derive a perturbative low-energy theory suitable to describe the quantum antiferromagnetic phase (AF) as a function of hole doping. At half-filling, we deal with the underlying spin degrees of freedom of the quantum AF Heisenberg model by employing a second-order spin-wave analysis, in which case we have calculated the ground-state energy and the staggered magnetization; the results are in very good agreement with previous studies. Further, in the continuum, we derive a nonlinear σ model with a topological Hopf term that describes the AF-VBS (valence bond solid) competition. Lastly, in the challenging doped regime, our approach allows the derivation of a t-J Hamiltonian, and the analysis of the role played by charge and spin quantum fluctuations on the ground-state energy and, particularly, on the breakdown of the AF order at a critical hole doping; the results are benchmarked against recent Grassmann tensor product state simulations.

DOI: 10.1103/PhysRevB.92.045105 PACS number(s): 71.10.Fd, 75.10.Lp, 72.80.Vp, 73.22.Pr

I. INTRODUCTION

In the last decade, the physics of electronic correlation in honeycomb and hexagonal lattice materials has been the issue of extensive theoretical and experimental investigations [1]. Indeed, in view of quite recent experimental activities, it has been reported that the undoped $Cu^{2+}(3d^9)$ spin-$\frac{1}{2}$ compound $In_3Cu_2VO_9$ [2–4] displays an antiferromagnetic Néel (AF) ground state. Likewise, experimental evidence has been provided that the undoped materials $Na_3T_2SbO_6$ [5], with $T = Cu^{2+}$; $T = Ni^{2+}$ ($3d^9 4s^1$; $S = 1$), and $T = Co^{2+}$ ($3d^7$; $S = 3/2$) also exhibit AF order. Moreover, experimental data have also indicated that Li_2RuO_3 [6] presents valence bond solid (VBS) or liquid phase; whereas it has been observed that Na_2IrO_3 [7] displays an AF Mott-insulating ground state.

On the theoretical side, various attempts have been undertaken with the purpose of describing the underlying mechanisms governing the physical properties of these materials. In the context of the Heisenberg model, the occurrence of an AF ground state on the honeycomb lattice at half-filling has been studied via quantum Monte Carlo (QMC) simulations [8,9], the second-order spin-wave perturbation theory [10], series expansion [11], tensor product state (TPS) numerical calculations [12,13] and Grassmann tensor product state (GTPS) numerical studies [14]. Also, the Hubbard model at half-filling [15] and generalized (competitive interactions) Heisenberg models [16] have been used with the aim of describing the possible occurrence of a VBS ground state [17–20]. Additionally, it has been shown that the AF-VBS competition takes place within the framework of the theory of unconventional quantum critical points [21–24]. However, we remark that in the context of the Hubbard model detailed QMC studies [25] at half-filling have excluded the occurrence of a VBS or liquid phase, while a robust AF phase was predicted to occur in the strong-coupling regime (Heisenberg limit).

On the other hand, of special interest are doped Mott insulators, notably its link with the physics of high-temperature superconductivity [26–28]. In a broader perspective, the t-J model has provided a comprehensive framework for investigating the effect of charge and spin quantum fluctuations on doped Mott insulators [26–28]. Recently, a numerical analysis through GTPS [14] calculations of the t-J model on the honeycomb lattice has been reported, in particular the data concerning the breakdown of the AF order due to hole doping. Despite all these relevant contributions, including the mean-field, random phase approximation (RPA) [29], and nonlinear σ model [30] studies, to the best of our knowledge, no analytical approach (in a controllable quantitative perturbative scheme) has been reported to describe the interplay between charge and spin quantum fluctuations in the Hubbard model on the honeycomb lattice, and the consequent destruction of the AF phase in the hole-doped regime.

In this work, we present a systematic and comprehensive analytical study of the strongly coupled Hubbard model on the honeycomb lattice at half-filling and in the hole-doped regime within a unifying functional-integral framework. The remaining part of the paper is organized as follows: In Sec. II, we establish the functional-integral representation in terms of Grassmann fields (charge degrees of freedom) and SU(2) gauge fields (spin degrees of freedom). In Sec. III, the Hamiltonian associated with the charge degrees of freedom is exactly diagonalized. The electronic dispersion exhibits a gap due to the Coulomb repulsive interaction, while in the tight-binding case we obtain the well known Dirac-like spectrum. In Sec. IV, we derive a perturbative low-energy Lagrangian density suitable to describe both the half-filling and doped regimes. Section V is devoted to the half-filling case,

in which case the large-U Hubbard model is mapped onto the quantum Heisenberg model described by SU(2) gauge fields. Further, in Appendix, the continuum limit of the referred model is mapped onto the nonlinear σ model with a topological Hopf term, which describes the AF-VBS competition. In Sec. VI, we focus on the hole-doped regime. This most challenging topic is studied within a controllable perturbative scheme, which allows us to unveil the role played by charge and spin quantum fluctuations in the breakdown of the hole-doped AF phase. Finally, concluding remarks are presented in Sec. VII.

II. FUNCTIONAL-INTEGRAL REPRESENTATION

The Hamiltonian of the Hubbard model on the honeycomb lattice reads

$$\mathcal{H} = -t \sum_{\langle i\alpha, j\beta\rangle\sigma} (\hat{c}^{\dagger}_{i\alpha\sigma}\hat{c}_{j\beta\sigma} + \hat{c}^{\dagger}_{j\beta\sigma}\hat{c}_{i\alpha\sigma}) + U \sum_{i\alpha} \hat{n}_{i\alpha\uparrow}\hat{n}_{i\alpha\downarrow}, \tag{1}$$

where $\hat{c}^{\dagger}_{i\alpha\sigma}$ ($\hat{c}_{i\alpha\sigma}$) denotes the creation (annihilation) fermion operator of spin σ ($=\uparrow,\downarrow$) on one of the inequivalent site $\alpha =$ A or B of a unit cell $\boldsymbol{i} = 1,\ldots,N_c$, with $N_c(N/2)$ being the number of unit cells (sites) [see Fig. 1(a)]; $\hat{n}_{i\alpha\sigma} = \hat{c}^{\dagger}_{i\alpha\sigma}\hat{c}_{i\alpha\sigma}$ is the electron number operator with spin σ at the position $\boldsymbol{i}\alpha$. The first term describes hopping of electrons with kinetic energy t between nearest-neighbor sites of distinct sublattices, and the second one is the on-site Coulombian repulsive interaction $U > 0$. We remark that the version of the Hubbard model in Eq. (1) offers an effective means for a proper description of the

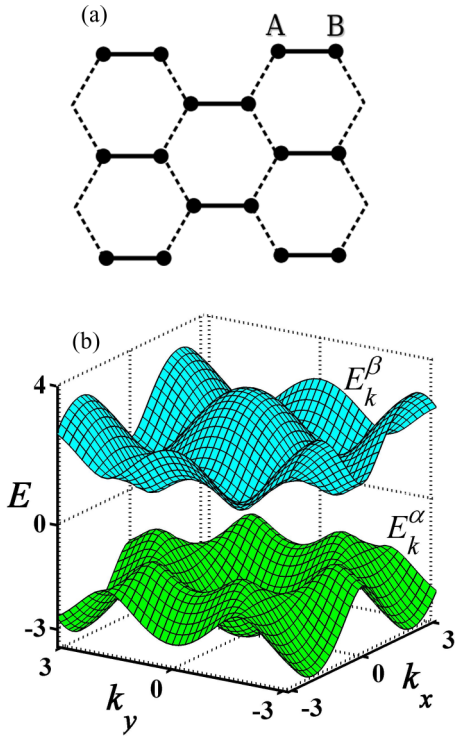

FIG. 1. (Color online) (a) Honeycomb lattice in real space with the two inequivalent A and B lattice sites of a unit cell. (b) Energy spectrum (in units of t) of the charge Hamiltonian [Eq. (24)] on the honeycomb lattice, with a Hubbard charge gap U.

magnetic properties of the copper oxide compounds mentioned in Introduction.

Usually, the interaction term in Eq. (1) is treated by means of the so-called Hubbard-Stratonovich transformation [31], which has been used to develop the functional-integral representation of the Hubbard model suitable to describe diagrammatic perturbation theory [32], critical phenomena [33] in 3D, and magnetic [34,35], and superconducting [36] properties in 2D.

On the other hand, in the context of the large-U Hubbard model in 1D [37] and quasi-1D [38], it has been shown that this term can also be treated through the use of a decomposition procedure. Hence we handle the particle density product in Eq. (1) by means of such a decomposition procedure [37,38], which consist in expressing $\hat{n}_{i\alpha\uparrow}\hat{n}_{i\alpha\downarrow}$ in terms of charge and spin operators:

$$\hat{n}_{i\alpha\uparrow}\hat{n}_{i\alpha\downarrow} = \tfrac{1}{2}\hat{\rho}_{i\alpha} - 2(\hat{\boldsymbol{S}}_{i\alpha}\cdot\boldsymbol{n}_{i\alpha})^2, \tag{2}$$

where $\hat{\rho}_{i\alpha} = \hat{n}_{i\alpha\uparrow} + \hat{n}_{i\alpha\downarrow}$, and $\hat{\boldsymbol{S}}_{i\alpha} = 1/2\sum_{\sigma\sigma'}\hat{c}^{\dagger}_{i\alpha\sigma'}\boldsymbol{\sigma}_{\sigma'\sigma}\hat{c}_{i\alpha\sigma}$, are the charge-density and the spin-1/2 operators, respectively, $\boldsymbol{\sigma}_{\sigma'\sigma}$ denotes the Pauli matrix elements ($\hbar \equiv 1$), and $\boldsymbol{n}_{i\alpha}$ is a unit vector field along the spin-quantization axis of an electron at site $i\alpha$. In addition, since the expectation value of the local charge-density operator is 0, 1, or 2, we can write down the formal relation

$$(\hat{\boldsymbol{S}}_{i\alpha}\cdot\boldsymbol{n}_{i\alpha})^2 = \frac{\rho_{i\alpha}(2-\rho_{i\alpha})}{4}, \tag{3}$$

which is consistent with the fact that the expectation value of the operator on the left-hand side of the above equation is $\langle(\hat{\boldsymbol{S}}_{i\alpha}\cdot\boldsymbol{n}_{i\alpha})^2\rangle = (\pm 1/2)^2 = 1/4$. Hence we have formally established that

$$\hat{\boldsymbol{S}}_{i\alpha}\cdot\boldsymbol{n}_{i\alpha} = p_{i\alpha}\frac{\rho_{i\alpha}(2-\rho_{i\alpha})}{2}, \tag{4}$$

where the staggered factor $p_{i\alpha}$ is conveniently chosen to be $p_{i\alpha} = 1$ at the A sites with spin-up ($\sigma =\uparrow$), and $p_{i\alpha} = -1$ at the B sites with spin-down ($\sigma =\downarrow$). This choice anticipates the occurrence of a long-range AF ground state at half-filled band. Furthermore, let us define the normalized weight function: $\int\prod_{i\alpha} d^2\boldsymbol{n}_{i\alpha} W(\boldsymbol{n}_{i\alpha}) = 1$, where $W(\boldsymbol{n}_{i\alpha}) = \sqrt{\frac{\varphi}{\pi}}\exp\{-\varphi[\boldsymbol{S}_{i\alpha}\cdot\boldsymbol{n}_{i\alpha} - \frac{p_{i\alpha}}{2}\rho_{i\alpha}(2-\rho_{i\alpha})]^2\}$ and $\varphi\to\infty$ (delta-like limit).

In order to determine the partition function

$$\mathcal{Z} = \mathrm{Tr}[\exp(-\beta\mathcal{H})] \tag{5}$$

at a temperature $k_BT = 1/\beta$, we are going to use the standard procedure [39–41], i.e., we formally slice the continuous imaginary time $\tau\in[0,\beta)$ into M finite discrete intervals $[\tau_r,\tau_{r+1})$ of equal size $\delta\tau$, where $r = 0,1,\ldots,M-1, \tau_0 = 0$, $\tau_M = \beta$, and $\beta = M\delta\tau$. Thus, by considering the limits $M\to\infty, \delta\tau\to 0$, and using the Trotter formula, we can write down $\mathcal{Z}$ as

$$\mathcal{Z} = \mathrm{Tr}\left\{\hat{T}\prod_{r=0}^{M-1}\exp[-\delta\tau\mathcal{H}(\tau_r)]\right\}, \tag{6}$$

where $\hat{T}$ is the time-ordering operator. We now introduce, between each time interval, an overcomplete basis of fermionic coherent states, $1 = \int\prod_{i\alpha\sigma} dc^{\dagger}_{i\alpha\sigma}dc_{i\alpha\sigma}\exp$

$(-c^{\dagger}_{i\alpha\sigma}c_{i\alpha\sigma})|c_{i\alpha\sigma}\rangle\langle c_{i\alpha\sigma}|$, where $\{c^{\dagger}_{i\alpha\sigma},c_{i\alpha\sigma}\}$ denotes a set of Grassmann fields satisfying antiperiodic boundary conditions in the imaginary-time domain: $c^{\dagger}_{i\alpha\sigma}(0)=-c^{\dagger}_{i\alpha\sigma}(\beta)$ and $c_{i\alpha\sigma}(0)=-c_{i\alpha\sigma}(\beta)$, while the unit vector field satisfies periodic ones: $\boldsymbol{n}_{i\alpha}(0)=\boldsymbol{n}_{i\alpha}(\beta)$. Thereby, the partition function takes the form

$$\mathcal{Z}=\int\prod_{i\alpha}\mathcal{D}^2\boldsymbol{n}_{i\alpha}\prod_{i\alpha}\mathcal{D}c^{\dagger}_{i\alpha}\mathcal{D}c_{i\alpha}\exp\left[-\int_0^{\beta}\mathcal{L}(\tau)d\tau\right], \quad (7)$$

where the measures are defined by $\mathcal{D}^2\boldsymbol{n}_{i\alpha}\equiv\lim_{M\to\infty}\prod_{r=0}^{M-1}d^2\boldsymbol{n}_{i\alpha}(\tau_r)W[\boldsymbol{n}_{i\alpha}(\tau_r)]$, $\mathcal{D}c^{\dagger}_{i\alpha\sigma}\mathcal{D}c_{i\alpha\sigma}\equiv\lim_{M\to\infty}\prod_{r=0}^{M-1}dc^{\dagger}_{i\alpha\sigma}(\tau_r)dc_{i\alpha\sigma}(\tau_r)$, and $\mathcal{L}(\tau)$ reads

$$\mathcal{L}(\tau)=\sum_{i\alpha\sigma}c^{\dagger}_{i\alpha\sigma}\partial_\tau c_{i\alpha\sigma}-t\sum_{\langle i\alpha,j\beta\rangle\sigma}(c^{\dagger}_{i\alpha\sigma}c_{j\beta\sigma}+c^{\dagger}_{j\beta\sigma}c_{i\alpha\sigma})+U\sum_{i\alpha}\left[\frac{1}{2}\rho_{i\alpha}-p_{i\alpha}(\boldsymbol{S}_{i\alpha}\cdot\boldsymbol{n}_{i\alpha})\right]. \quad (8)$$

At this stage, it is interesting to consider the symmetry exhibited by the AF order. Here, we shall use a SU(2) matrix [42], where the group parameter space is the surface of the unit S^3 sphere, parametrized according to the symmetry displayed by the AF phase. As the unit vector $\boldsymbol{n}_{i\alpha}$, i.e., the Néel order parameter, lies in the manifold S^2, the corresponding SU(2) matrix, $U_{i\alpha}$, assumes the form

$$U_{i\alpha}=\begin{bmatrix}\cos\left(\frac{\theta_{i\alpha}}{2}\right) & -\sin\left(\frac{\theta_{i\alpha}}{2}\right)e^{-i\phi_{i\alpha}}\\ \sin\left(\frac{\theta_{i\alpha}}{2}\right)e^{i\phi_{i\alpha}} & \cos\left(\frac{\theta_{i\alpha}}{2}\right)\end{bmatrix}, \quad (9)$$

where $\theta_{i\alpha}$ is the polar angle between the z axis and the unit vector $\boldsymbol{n}_{i\alpha}$, and $\phi_{i\alpha}$ is an arbitrary azimuth angle due to the U(1) gauge freedom. Moreover, it obeys the relation $U^{\dagger}_{i\alpha}(\hat{\sigma}\cdot\boldsymbol{n}_{i\alpha})U_{i\alpha}=\sigma^z$, which explicitly manifest the rotationally broken symmetry along the z axis. Notice also that by taking $\theta_{iA}=\theta_{iB}=0$, together with the proper choice of the staggered factor $p_{i\alpha}$, one obtains the representation for the classical Néel order. In this context, it will prove very useful to introduce a new set of Grassmann fields, $\{a^{\dagger}_{i\alpha\sigma},a_{i\alpha\sigma}\}$, according to the transformation

$$a_{i\alpha\sigma}=\sum_{\sigma'}(U_{i\alpha})^{\dagger}_{\sigma\sigma'}c_{i\alpha\sigma'}, \quad (10)$$

whose associated spins point along the global z axis.

Correspondingly, with the help of Eqs. (9) and (10), the Lagrangian in Eq. (8) is transformed into the following form:

$$\mathcal{L}(\tau)=\sum_{i\alpha\sigma}a^{\dagger}_{i\alpha\sigma}\partial_\tau a_{i\alpha\sigma}+\sum_{i\alpha\sigma\sigma'}a^{\dagger}_{i\sigma'}(U_{i\alpha})^{\dagger}_{\sigma'\sigma}\partial_\tau(U_{i\alpha})_{\sigma'\sigma}a_{i\alpha\sigma}-t\sum_{\langle i\alpha,j\beta\rangle\sigma}(a^{\dagger}_{i\alpha\sigma}a_{j\beta\sigma}+\text{H.c.})-t\sum_{\langle i\alpha,j\beta\rangle\sigma\sigma'}[a^{\dagger}_{i\alpha\sigma'}(U^{\dagger}_{i\alpha}U_{j\beta}-1)_{\sigma'\sigma}a_{j\beta\sigma}+\text{H.c.}]+\frac{U}{2}\sum_{i\alpha\sigma}(1-p_{i\alpha}\sigma)a^{\dagger}_{i\alpha\sigma}a_{i\alpha\sigma}. \quad (11)$$

Remarkably, $\mathcal{L}(\tau)$ can be split up into two parts. One with only charge degrees of freedom:

$$\mathcal{L}_0=\sum_{i\alpha\sigma}a^{\dagger}_{i\alpha\sigma}\partial_\tau a_{i\alpha\sigma}-t\sum_{\langle i\alpha,j\beta\rangle\sigma}(a^{\dagger}_{i\alpha\sigma}a_{j\beta\sigma}+\text{H.c.})+\frac{U}{2}\sum_{i\alpha\sigma}(1-p_{i\alpha}\sigma)a^{\dagger}_{i\alpha\sigma}a_{i\alpha\sigma}, \quad (12)$$

and the other describes the coupling between the charge (Grassmann fields $a^{\dagger}_{i\alpha\sigma}$ and $a_{i\alpha\sigma}$) and spin degrees of freedom [SU(2) gauge fields $U_{i\alpha}$]:

$$\mathcal{L}_n=\sum_{i\alpha\sigma\sigma'}a^{\dagger}_{i\alpha\sigma'}(U_{i\alpha})^{\dagger}_{\sigma'\sigma}\partial_\tau(U_{i\alpha})_{\sigma'\sigma}a_{i\alpha\sigma}-t\sum_{\langle i\alpha,j\beta\rangle\sigma\sigma'}[a^{\dagger}_{i\alpha\sigma'}(U^{\dagger}_{i\alpha}U_{j\beta}-1)_{\sigma'\sigma}a_{j\beta\sigma}+\text{H.c.}]. \quad (13)$$

III. ANALYSIS OF CHARGE DEGREES OF FREEDOM IN $\mathcal{L}_0$

We now turn our attention to $\mathcal{L}_0$ in Eq. (12). By performing the Legendre transform

$$\mathcal{H}_0=-\sum_{i\alpha\sigma}\frac{\partial\mathcal{L}_0}{\partial(\partial_\tau a_{i\alpha\sigma})}\partial_\tau a_{i\alpha\sigma}+\mathcal{L}_0, \quad (14)$$

where

$$\frac{\partial\mathcal{L}_0}{\partial(\partial_\tau a_{i\alpha\sigma})}=a^{\dagger}_{i\alpha\sigma}, \quad (15)$$

we get the Hamiltonian associated with the charge degrees of freedom:

$$\mathcal{H}_0=-t\sum_{\langle i\alpha,j\beta\rangle\sigma}(a^{\dagger}_{i\alpha\sigma}a_{j\beta\sigma}+\text{H.c.})+\frac{U}{2}\sum_{i\alpha\sigma}(1-p_{i\alpha}\sigma)a^{\dagger}_{i\alpha\sigma}a_{i\alpha\sigma}. \quad (16)$$

In order to diagonalize $\mathcal{H}_0$ we need a two step procedure. Initially, we perform a Fourier transform

$$a_{\boldsymbol{k}\sigma}=\frac{1}{\sqrt{N_c}}\sum_i e^{i\boldsymbol{k}\cdot\boldsymbol{i}}a_{i\sigma},\qquad b_{\boldsymbol{k}\sigma}=\frac{1}{\sqrt{N_c}}\sum_j e^{-i\boldsymbol{k}\cdot\boldsymbol{j}}b_{j\sigma}, \quad (17)$$

where $a_{\boldsymbol{k}\sigma}$ ($b_{\boldsymbol{k}\sigma}$) is the Fourier transform of the Grassmann fields associated with the A (B) sublattice, i.e., for notation convenience we have replaced $a_{j\beta\sigma}\to b_{j\sigma}$; in addition, we introduce the new set of Grassmann fields [43]:

$$A_{\boldsymbol{k}\sigma}=\frac{a_{\boldsymbol{k}\sigma}}{\sqrt{2}}+\frac{w^*_{\boldsymbol{k}}}{\sqrt{2}|w_{\boldsymbol{k}}|}b_{\boldsymbol{k}\sigma}, \quad (18)$$

$$B_{\boldsymbol{k}\sigma}=\frac{a_{\boldsymbol{k}\sigma}}{\sqrt{2}}-\frac{w^*_{\boldsymbol{k}}}{\sqrt{2}|w_{\boldsymbol{k}}|}b_{\boldsymbol{k}\sigma}, \quad (19)$$

where

$$w^*_{\boldsymbol{k}}=e^{-ik_x}+2e^{i\frac{k_x}{2}}\cos\left(\frac{\sqrt{3}k_y}{2}\right). \quad (20)$$

Therefore one obtains

$$\mathcal{H}_0 = -\sum_{k\sigma}\epsilon_k(A^\dagger_{k\sigma}A_{k\sigma} - B^\dagger_{k\sigma}B_{k\sigma}) + \frac{U}{4}\sum_{k\sigma}(1-\sigma) \times (A^\dagger_{k\sigma}A_{k\sigma} + A^\dagger_{k\sigma}B_{k\sigma} + B^\dagger_{k\sigma}A_{k\sigma} + B^\dagger_{k\sigma}B_{k\sigma}), \tag{21}$$

in which

$$\epsilon_k = t\sqrt{3 + 2\cos(\sqrt{3}k_y) + 4\cos\left(\frac{3k_x}{2}\right)\cos\left(\frac{\sqrt{3}k_y}{2}\right)}. \tag{22}$$

Now, we can diagonalize $\mathcal{H}_0$ in Eq. (21) by means of the Bogoliubov transformation:

$$A_{k\sigma} = u_k\alpha_{k\sigma} - \sigma v_k\beta_{k\sigma}; \quad B_{k\sigma} = \sigma v_k\alpha_{k\sigma} + u_k\beta_{k\sigma}, \tag{23}$$

restricted by the canonical constraint $(u_k)^2 + (v_k)^2 = 1$; as a result, the diagonal form of $\mathcal{H}_0$ reads

$$\mathcal{H}_0 = \sum_{k\sigma}\left(E^\alpha_k\alpha^\dagger_{k\sigma}\alpha_{k\sigma} + E^\beta_k\beta^\dagger_{k\sigma}\beta_{k\sigma}\right), \tag{24}$$

where

$$u_k = \frac{1}{\sqrt{2}}\sqrt{1 + \frac{|\epsilon_k|}{E_k}}; \quad v_k = \frac{1}{\sqrt{2}}\sqrt{1 - \frac{|\epsilon_k|}{E_k}}, \tag{25}$$

with

$$E_k = \sqrt{\epsilon_k^2 + \frac{U^2}{4}}; \quad E^{\alpha,\beta}_k = \mp E_k + U/2. \tag{26}$$

The Hamiltonian in Eq. (24) presents two dispersive bands: the low-energy ($\alpha_{k\sigma}$) and the high-energy one ($\beta_{k\sigma}$), split up by the Hubbard gap U, as shown in Fig. 1(b).

Finally, it should be noted that the noninteracting tight-binding spectrum of $\mathcal{H}_0$ can be recast by setting $U = 0$. In fact, these two dispersive bands meet in the so-called Dirac points. As it is well known, close to the Dirac points the system can be mapped onto free massless Dirac fermions [1].

IV. EFFECTIVE LAGRANGIAN DENSITY IN THE STRONG-COUPLING REGIME

In this section, we shall build a strong-coupling ($U/t \gg 1$) perturbative low-energy theory (effective Lagrangian density) suitable to describe the system in the half-filled and doped regimes. Our aim is to investigate the relevant processes that characterize the AF order in the large-U regime in terms of the lower α band and the upper β band (see Fig. 1).

Let us start by expanding the auxiliary functions u_k and v_k in Eq. (25) in powers of t/U as follows:

$$u_k = \frac{1}{\sqrt{2}}\left[1 + \frac{t|w_k|}{U} - \frac{t^2|w_k|^2}{2U^2} + \mathcal{O}\left(\frac{t^3}{U^3}\right)\right],$$
$$v_k = \frac{1}{\sqrt{2}}\left[1 - \frac{t|w_k|}{U} - \frac{t^2|w_k|^2}{2U^2} + \mathcal{O}\left(\frac{t^3}{U^3}\right)\right], \tag{27}$$

where $\epsilon_k = t|w_k|$ [see Eq. (20)]. In the sequence, by using Eqs. (17)–(19) and (23), we can express the Grassmann field $a_{i\alpha\sigma}$ in terms of the Bogoliubov fields $\alpha_{k\sigma}$ and $\beta_{k\sigma}$:

$$a_{i\alpha\sigma} = \frac{1}{\sqrt{N_c}}\sum_{k\sigma}e^{i\boldsymbol{k}\cdot\boldsymbol{i}}[(u_k + \sigma v_k)\alpha_{k\sigma} + (u_k - \sigma v_k)\beta_{k\sigma}]. \tag{28}$$

Now, by substituting Eq. (27) into Eq. (28), we can obtain a perturbative expression for the Grassmann field $a_{i\alpha\sigma}$ in terms of the spinless Grassmann fields α_i and β_i (see below), up to $\mathcal{O}(t^2/U^2)$, as follows:

$$a_{i\alpha\sigma} = \theta(\sigma)\alpha_i + \theta(-\sigma)\beta_i + \theta(-\sigma)\frac{t}{U}\alpha_i + \theta(\sigma)\frac{t}{U}\beta_i - \frac{t^2}{U^2}\left[\theta(-\sigma)\sum_j(\alpha_{i+\hat{\boldsymbol{e}}_j} + \alpha_{i-\hat{\boldsymbol{e}}_j}) + 3\theta(\sigma)\alpha_i\right] + \frac{t^2}{U^2}\left[\theta(\sigma)\sum_j(\beta_{i+\hat{\boldsymbol{e}}_j} + \beta_{i-\hat{\boldsymbol{e}}_j}) + 3\theta(-\sigma)\beta_i\right], \tag{29}$$

where α_i and β_i are defined by [37]

$$\alpha_i = \sqrt{\frac{1}{N_c}}\sum_\sigma\theta(\sigma)\sum_k e^{i\boldsymbol{k}\cdot\boldsymbol{i}}\alpha_{k\sigma},$$
$$\beta_i = \sqrt{\frac{1}{N_c}}\sum_\sigma\theta(-\sigma)\sum_k e^{i\boldsymbol{k}\cdot\boldsymbol{i}}\beta_{k\sigma}, \tag{30}$$

$\theta(\sigma)$ is the Heaviside function, with $\theta(\sigma)\theta(-\sigma') = \theta(\sigma)\delta_{\sigma,-\sigma'}$, and $\hat{\boldsymbol{e}}_j$ are the standard three unit vectors of the honeycomb lattice [1]. This representation is appropriated to describe the AF order, in the large-U regime, in the context of the referred α and β bands. For example, to $\mathcal{O}(t/U)$, Eq. (29) yields $a_{iA\uparrow} \approx \alpha_i$ and $a_{iB\downarrow} \approx \alpha_i$, which is consistent with the two AF sublattice sites in a given unit cell $\boldsymbol{i}$ (low-energy spin configuration), while for the high-energy β band, one finds an opposite spin configuration: $a_{iA\downarrow} \approx \beta_i$ and $a_{iB\uparrow} \approx \beta_i$.

At this stage, by inserting Eq. (29) into Eq. (16), and keeping terms up to $\mathcal{O}(J \equiv 4t^2/U)$, one can write $\mathcal{H}_0$ in terms of the spinless Grassmann fields α_i and β_i in direct space:

$$\mathcal{H}_0 = -J\sum_i(\alpha^\dagger_i\alpha_i - \beta^\dagger_i\beta_i) + U\sum_i\beta^\dagger_i\beta_i - \frac{J}{8}\sum_{ij}(\alpha^\dagger_i\alpha_{i+\hat{\boldsymbol{e}}_j} - \beta^\dagger_i\beta_{i+\hat{\boldsymbol{e}}_j} + \text{H.c.}). \tag{31}$$

The charge Hamiltonian above correctly exhibits the phenomenon of band shrinking [44] in the large-U regime. Notwithstanding, we stress that $\mathcal{H}_0$ describe only processes in the charge sector, i.e., no spin dynamics is involved. Therefore, in our study of the magnetic properties of the system, these processes play no role and, after a Legendre transform, the Lagrangian density can be taken simply as

$$\mathcal{L}_0 = \sum_i\alpha^\dagger_i\partial_\tau\alpha_i, \tag{32}$$

where the dynamic (kinetic) term signals the background of the charge degrees of freedom.

We now employ the same perturbative scheme to $\mathcal{L}_n$, i.e., we insert Eq. (29) into Eq. (13), such that, by keeping terms which incorporates only the most relevant low-energy processes, i.e., quantum charge and spin dynamics between nearest-neighbor sites, we obtain the following perturbative expansion for $\mathcal{L}_n$:

$$\mathcal{L}_n = \sum_{i\alpha\sigma} \theta(\sigma)(U^\dagger_{i\alpha}\partial_\tau U_{i\alpha})_{\sigma\sigma}\alpha^\dagger_i\alpha_i - t\sum_{ij\alpha\beta\sigma}[\theta(-\sigma)(U^\dagger_{i\alpha}U_{i+\hat{e}_j\beta}-1)_{\sigma,-\sigma}\alpha^\dagger_i\alpha_{i+\hat{e}_j}+\text{H.c.}]$$
$$+\frac{t}{2U}\sum_{ij\alpha\sigma}[\theta(-\sigma)(U^\dagger_{i\alpha}\partial_\tau U_{i\alpha})_{\sigma,-\sigma}(\alpha^\dagger_{i+\hat{e}_j}+\alpha^\dagger_{i-\hat{e}_j})\alpha_i+\text{H.c.}]$$
$$-t\sum_{ij\alpha\beta\sigma}\{(U^\dagger_{i\alpha}U_{i+\hat{e}_j\beta}-1)_{\sigma\sigma}[\theta(\sigma)\alpha^\dagger_i\beta_{i+\hat{e}_j}-\theta(\sigma)\beta^\dagger_i\alpha_{i+\hat{e}_j}]+\text{H.c.}\}. \tag{33}$$

It should be noted that the last term in Eq. (33) contains hopping between α and β bands. This term must be treated perturbatively, so that $\mathcal{L}_n$ appears as dependent on the low-energy α band only. We thus consider the perturbing Hamiltonian below:

$$\mathcal{H}_1 = -t\sum_{ij\alpha\beta\sigma}\{(U^\dagger_{i\alpha}U_{i+\hat{e}_j\beta}-1)_{\sigma\sigma}[\theta(\sigma)\beta^\dagger_i\alpha_{i+\hat{e}_j}-\theta(\sigma)\alpha^\dagger_i\beta_{i+\hat{e}_j}]+\text{H.c.}\}. \tag{34}$$

It can be handled by means of standard second-order perturbation theory [38,45], which is consistent with the strong-coupling expansion up to $\mathcal{O}(t^2/U)$:

$$\Delta E \equiv \mathcal{H}_{\text{eff}} = \sum_{k\sigma}\frac{|\langle\alpha_{k\sigma}|\mathcal{H}_1|\beta_{k\sigma}\rangle|^2}{E^\alpha_k - E^\beta_k}, \tag{35}$$

where the unperturbed state is the system at half-filling: the low-energy α band is filled, while the β band is empty. As a consequence, the shift in the energy ΔE due to $\mathcal{H}_1$ corresponds to an effective Hamiltonian, $\mathcal{H}_{\text{eff}}$, expressed in terms of the low-energy α band only:

$$\mathcal{H}_{\text{eff}} = -\frac{t^2}{2U}\sum_{ij\alpha\beta\sigma}\theta(\sigma)\left[\left|\left(U^\dagger_{i\alpha}U_{i+\hat{e}_j\beta}\right)_{\sigma\sigma}\right|^2+\left|\left(U^\dagger_{i\alpha}U_{i-\hat{e}_j\beta}\right)_{\sigma\sigma}\right|^2\right]\alpha^\dagger_i\alpha_i. \tag{36}$$

The above result allow us to obtain a perturbative expression of $\mathcal{L}_n$ in terms of the low-energy α band only.

Correspondingly, by adding $\mathcal{L}_0$ [see Eq. (32)] to the perturbation expression of $\mathcal{L}_n$, we find that the effective low-lying Lagrangian density of the honeycomb Hubbard model in the large-U regime, up to $\mathcal{O}(J)$, is given by

$$\mathcal{L} = \sum_i \alpha^\dagger_i\partial_\tau\alpha_i + \sum_{i\alpha\sigma}\theta(\sigma)(U^\dagger_{i\alpha}\partial_\tau U_{i\alpha})_{\sigma\sigma}\alpha^\dagger_i\alpha_i - t\sum_{ij\alpha\beta\sigma}\left[\theta(-\sigma)\left(U^\dagger_{i\alpha}U_{i+\hat{e}_j\beta}\right)_{\sigma,-\sigma}\alpha^\dagger_i\alpha_{i+\hat{e}_j}+\text{H.c.}\right]$$
$$+\frac{J}{8t}\sum_{ij\alpha\sigma}(U^\dagger_{i\alpha}\partial_\tau U_{i\alpha})_{\sigma,-\sigma}\left[\theta(-\sigma)\alpha^\dagger_i\left(\alpha_{i+\hat{e}_j}+\alpha_{i-\hat{e}_j}\right)+\text{H.c.}\right]-\frac{J}{8}\sum_{ij\alpha\beta\sigma}\theta(\sigma)\left[\left|\left(U^\dagger_{i\alpha}U_{i+\hat{e}_j\beta}\right)_{\sigma\sigma}\right|^2+\left|\left(U^\dagger_{i\alpha}U_{i-\hat{e}_j\beta}\right)_{\sigma\sigma}\right|^2\right]\alpha^\dagger_i\alpha_i. \tag{37}$$

We emphasize that the above low-lying Lagrangian density incorporates only quadratic terms in $\alpha^\dagger$,α. We can thus integrate out the fermions degrees of freedom in order to explicit the spin structure embedded in $U^\dagger_{i\alpha}U_{i+\hat{e}_j\alpha}$ and $U^\dagger_{i\alpha}\partial_\tau U_{i\alpha}$.

V. HEISENBERG MODEL AND QUANTUM SPIN FLUCTUATIONS

In the half-filled regime, the charge degrees of freedom are frozen ($\langle\alpha^\dagger_i\partial_\tau\alpha_i\rangle = 0$ and $\langle\alpha^\dagger_i\alpha_{i+\hat{e}_j}\rangle = 0$), i.e., the lower-energy α band is completely filled by electrons: $n_\alpha \equiv \langle\alpha^\dagger_i\alpha_i\rangle = 1$. Accordingly, it turns out that only the spin degrees of freedom survive and are described by the SU(2) gauge fields in Eq. (37). Further, this localized electronic background allows the emergence of an AF phase [15,25]. Indeed, by performing the following Legendre transform:

$$\mathcal{H}^s = -\sum_{i\alpha\sigma}\frac{\partial\mathcal{L}}{\partial(\partial_\tau U_{i\alpha})_{\sigma\sigma}}(\partial_\tau U_{i\alpha})_{\sigma\sigma}+\mathcal{L}, \tag{38}$$

where

$$\frac{\partial\mathcal{L}}{\partial(\partial_\tau U_{i\alpha})_{\sigma\sigma}} = \theta(\sigma)(U^\dagger_{i\alpha})_{\sigma\sigma}, \tag{39}$$

we can map the large-U Hubbard model, in the half-filling limit of the effective Lagrangian density in Eq. (37), onto the following Heisenberg-like Hamiltonian written in terms of the SU(2) gauge fields:

$$\mathcal{H}^s = -\frac{J}{8}\sum_{ij\alpha\beta\sigma}\theta(\sigma)\left[\left|\left(U^\dagger_{i\alpha}U_{i+\hat{e}_j\beta}\right)_{\sigma\sigma}\right|^2+\left|\left(U^\dagger_{i\alpha}U_{i-\hat{e}_j\beta}\right)_{\sigma\sigma}\right|^2\right]. \tag{40}$$

In fact, with the help of Eq. (9), we can write [38]

$$\left|\left(U^{\dagger}_{i\alpha}U_{i+\hat{\boldsymbol{e}}_j\beta}\right)_{\sigma\sigma}\right|^2 = \left[1+\cos(\theta_{i\alpha})\cos\left(\theta_{i+\hat{\boldsymbol{e}}_j\beta}\right) + \sin(\theta_{i\alpha})\sin\left(\theta_{i+\hat{\boldsymbol{e}}_j\beta}\right)\cos\left(\phi_{i\alpha}-\phi_{i+\hat{\boldsymbol{e}}_j\beta}\right)\right] \quad (41)$$

or

$$\left|\left(U^{\dagger}_{i\alpha}U_{i+\hat{\boldsymbol{e}}_j\beta}\right)_{\sigma\sigma}\right|^2 = \tfrac{1}{2}\left(1+\boldsymbol{n}_{i\alpha}\cdot\boldsymbol{n}_{i+\hat{\boldsymbol{e}}_j\beta}\right), \quad (42)$$

where $\boldsymbol{n}_{i\alpha} = \sin(\theta_{i\alpha})[\cos(\phi_{i\alpha})\hat{\boldsymbol{x}} + \sin(\phi_{i\alpha})\hat{\boldsymbol{y}}] + \cos(\theta_{i\alpha})\hat{\boldsymbol{z}}$ is the unit vector. Accordingly, $\mathcal{H}^s$ can be brought to its standard form:

$$\mathcal{H}^s = -J\sum_{ij\alpha\beta}\boldsymbol{S}_{i\alpha}\cdot\boldsymbol{S}_{i+\hat{\boldsymbol{e}}_j\beta} - h\sum_{i\alpha}\boldsymbol{S}_{i\alpha} + h\sum_{ij\beta}\boldsymbol{S}_{i+\hat{\boldsymbol{e}}_j\beta}, - \frac{zNJ}{8}, \quad (43)$$

where $\boldsymbol{S}_{i\alpha} = \boldsymbol{n}_{i\alpha}/2$, z is the coordination number ($z=3$ for the honeycomb lattice) and the two additional Zeeman terms (h is the magnetic field) allow us to perform the calculation of the staggered magnetization.

The second-order spin-wave theory [10] can offer an accurate description of the relevant physical quantities, such as the ground-state energy, E_0, and the staggered magnetization per site, m, which characterizes the AF order. In order to employ this method to the quantum AF Heisenberg model in Eq. (43) let us introduce the Holstein-Primakoff transformation:

$$\begin{aligned} S^z_{i\alpha} &= -a^{\dagger}_i a_i + S, \\ S^+_{i\alpha} &= \sqrt{2S - a^{\dagger}_i a_i}\, a_i, \\ S^-_{i\alpha} &= a^{\dagger}_i\sqrt{2S - a^{\dagger}_i a_i}, \end{aligned} \quad (44)$$

for an up-spin on A site of sublattice A, and

$$\begin{aligned} S^z_{i+\hat{\boldsymbol{e}}_j\beta} &= b^{\dagger}_{i+\hat{\boldsymbol{e}}_j} b_{i+\hat{\boldsymbol{e}}_j} - S, \\ S^+_{i+\hat{\boldsymbol{e}}_j\beta} &= \sqrt{2S - b^{\dagger}_{i+\hat{\boldsymbol{e}}_j} b_{i+\hat{\boldsymbol{e}}_j}}\, b_{i+\hat{\boldsymbol{e}}_j}, \\ S^-_{i+\hat{\boldsymbol{e}}_j\beta} &= b^{\dagger}_{i+\hat{\boldsymbol{e}}_j}\sqrt{2S - b^{\dagger}_{i+\hat{\boldsymbol{e}}_j} b_{i+\hat{\boldsymbol{e}}_j}}, \end{aligned} \quad (45)$$

for a neighboring down-spin of sublattice B; the bosonic creation and annihilation operators a_i and $a^{\dagger}_i$ obey the commutation relations: $[a_i, a^{\dagger}_{i'}] = \delta_{ii'}$ and $[b_j, b^{\dagger}_{j'}] = \delta_{jj'}$. Moreover, we apply the Fourier transform [see, e.g., Eq. (17)] together with the following Bogoliubov transformation:

$$\begin{aligned} a_{\boldsymbol{k}} &= \cosh(\theta_{\boldsymbol{k}})\alpha_{\boldsymbol{k}} - \sinh(\theta_{\boldsymbol{k}})\beta^{\dagger}_{\boldsymbol{k}}, \\ b_{\boldsymbol{k}} &= -\sinh(\theta_{\boldsymbol{k}})\alpha^{\dagger}_{\boldsymbol{k}} - \cosh(\theta_{\boldsymbol{k}})\beta_{\boldsymbol{k}}, \end{aligned} \quad (46)$$

where $\tanh(\theta_{\boldsymbol{k}}) = -\gamma_{\boldsymbol{k}}$ and the lattice structure factor $\gamma_{\boldsymbol{k}}$ reads

$$\gamma_{\boldsymbol{k}} \equiv \frac{1}{z}\sum_j e^{i\boldsymbol{k}\cdot\boldsymbol{e}_j} = \frac{1}{3}\left[e^{ik_x} + 2e^{-i\frac{k_x}{2}}\cos\left(\frac{\sqrt{3}k_y}{2}\right)\right]. \quad (47)$$

The resulting diagonalized Hamiltonian up to $\mathcal{O}(1/S^2)$, in $\boldsymbol{k}$-space, takes the form

$$\mathcal{H}^s = -\frac{zS^2JN}{2} + hSN + zSJ\sum_{\boldsymbol{k}}\left[\left(\sqrt{1-\gamma^2_{\boldsymbol{k}}}-1\right) + \sqrt{1-\gamma^2_{\boldsymbol{k}}}\left(\alpha^{\dagger}_{\boldsymbol{k}}\alpha_{\boldsymbol{k}} + \beta^{\dagger}_{\boldsymbol{k}}\beta_{\boldsymbol{k}}\right)\right] - \frac{zJ}{2N}\left[\sum_{\boldsymbol{k}}\left(\sqrt{1-\gamma^2_{\boldsymbol{k}}}-1\right)\right]^2 - h\sum_{\boldsymbol{k}}\left[\left(\frac{1}{\sqrt{1-\gamma^2_{\boldsymbol{k}}}}-1\right) + \frac{\alpha^{\dagger}_{\boldsymbol{k}}\alpha_{\boldsymbol{k}} + \beta^{\dagger}_{\boldsymbol{k}}\beta_{\boldsymbol{k}}}{\sqrt{1-\gamma^2_{\boldsymbol{k}}}}\right] - \frac{zJN}{8} - \frac{2zJ}{N}\sum_{\boldsymbol{k},\boldsymbol{k}'}\alpha^{\dagger}_{\boldsymbol{k}}\alpha_{\boldsymbol{k}}\beta^{\dagger}_{\boldsymbol{k}'}\beta_{\boldsymbol{k}'}. \quad (48)$$

Correspondingly, in the thermodynamic limit, the ground-state energy per site in the presence of a magnetic field becomes

$$\frac{E_h}{N} = -\frac{zS^2J}{2} + hS + \frac{zSJ}{4\pi^2}\int_{\mathrm{BZ}} d^2k\left(\sqrt{1-\gamma^2_{\boldsymbol{k}}}-1\right) - \frac{zJ}{32\pi^4}\left[\int_{\mathrm{BZ}} d^2k\left(\sqrt{1-\gamma^2_{\boldsymbol{k}}}-1\right)\right]^2 - \frac{h}{4\pi^2}\int_{\mathrm{BZ}} d^2k\left(\frac{1}{\sqrt{1-\gamma^2_{\boldsymbol{k}}}}-1\right) - \frac{zJ}{8}. \quad (49)$$

In the sequence, we take $S = 1/2$ and perform the integration over the first Brillouin zone (BZ): $|k_x| \leqslant 2\pi/3$ and $|k_y| \leqslant \pi/\sqrt{3}$. As a consequence, we have found that the ground-state energy per site at zero magnetic field is given by (we have subtracted the term $-zJ/8$ with the intention of comparing Eq. (49) at zero magnetic field to preceding results): $E_0/NJ \approx -0.5489$. Indeed, this result agrees very well with QMC [8,9] (-0.5440), second-order spin-wave analysis [10] (-0.5489), series expansion [11] (-0.5443), TPS [12,13] (-0.5445) and GTPS [14] (-0.5441) studies.

On the other hand, with the help of Eq. (49), we can straightforwardly derive the staggered magnetization per site: $m = \frac{1}{N}\frac{\partial E_h}{\partial h}|_{h=0}$. Thus one finds

$$m = S - \frac{1}{4\pi^2}\int_{\mathrm{BZ}} d^2k\left(\frac{1}{\sqrt{1-\gamma^2_{\boldsymbol{k}}}}-1\right), \quad (50)$$

which stands for both first- and second-order spin-wave perturbation theory. Further, the integration over the first BZ yields for $S = 1/2$: $m \approx 0.2418$, which is in good agreement with QMC results (0.22 ± 0.03 (Ref. [8]) and 0.2681(8) (Ref. [9]), second-order spin-wave theory [10] (0.2418), series expansion [11] [0.266(9)], and TPS simulations [0.2142 for the "virtual dimension" $D = 8$ (Ref. [12]), and 0.285 for $D \to \infty$

(Ref. [13])], while simulations using GTPS [14] predict slightly larger values: 0.3257 for $D = 10$ and 0.3239 for $D = 12$. Here, the "virtual dimension" D is a concept associated with the integer bond indices of classical tensor-networks on honeycomb lattices, and largely used in TPS and GTPS simulations [12–14]. Furthermore, it has been indicated, through topological arguments, the possible occurrence of a VBS phase on the honeycomb lattice [23]. Thus, in Appendix, we map the effective large-U Lagrangian density in Eq. (37), in the continuum limit, onto the quantum nonlinear σ model with a topological Hopf term, in which case its presence (Chern-Simons term) is crucial for the possible occurrence of a VBS order. However, despite that our results provide evidence for the existence of this topological term in the context of our approach, as mentioned in the Introduction, in the numerical studies of the Hubbard model at half-filling the VBS order did not appear as a stable phase [25].

VI. t-J MODEL: CHARGE AND SPIN QUANTUM FLUCTUATIONS

In this section, we provide a systematic study of the interplay between quantum charge and spin fluctuations in the breakdown of the AF order in the doped regime. In order to obtain the corresponding t-J Hamiltonian, let us apply the Legendre transform in Eq. (37):

$$\mathcal{H}^{t\text{-}J} = -\sum_{i}\frac{\partial\mathcal{L}}{\partial(\partial_\tau\alpha_i)}\partial_\tau\alpha_i - \sum_{ij\alpha\sigma}\frac{\partial\mathcal{L}}{\partial(\partial_\tau U_{i\alpha})_{\sigma\sigma}}(\partial_\tau U_{i\alpha})_{\sigma\sigma} - \sum_{ij\alpha\sigma}\frac{\partial\mathcal{L}}{\partial(\partial_\tau U_{i\alpha})_{\sigma,-\sigma}}(\partial_\tau U_{i\alpha})_{\sigma,-\sigma} + \mathcal{L}, \tag{51}$$

where

$$\frac{\partial\mathcal{L}}{\partial(\partial_\tau\alpha_i)} = \alpha_i^\dagger, \quad \frac{\partial\mathcal{L}}{\partial(\partial_\tau U_{i\alpha})_{\sigma\sigma}} = \theta(\sigma)(U_{i\alpha}^\dagger)_{\sigma\sigma}\alpha_i^\dagger\alpha_i, \quad \frac{\partial\mathcal{L}}{\partial(\partial_\tau U_{i\alpha})_{\sigma,-\sigma}} = \frac{J}{8t}(U_{i\alpha}^\dagger)_{\sigma,-\sigma}\left[\theta(-\sigma)\alpha_i^\dagger\left(\alpha_{i+\hat{e}_j}+\alpha_{i-\hat{e}_j}\right)+\text{H.c.}\right], \tag{52}$$

so that we indeed can map the large-U Hubbard model onto the following t-J Hamiltonian:

$$\mathcal{H}^{t\text{-}J} = -t\sum_{ij\alpha\beta\sigma}\left[\theta(-\sigma)\left(U_{i\alpha}^\dagger U_{i+\hat{e}_j\beta}\right)_{\sigma,-\sigma}\alpha_i^\dagger\alpha_{i+\hat{e}_j}+\text{H.c.}\right] - \frac{J}{8}\sum_{ij\alpha\beta\sigma}\theta(\sigma)\left[\left|\left(U_{i\alpha}^\dagger U_{i+\hat{e}_j\beta}\right)_{\sigma\sigma}\right|^2+\left|\left(U_{i\alpha}^\dagger U_{i+\hat{e}_j\beta}\right)_{\sigma\sigma}\right|^2\right]\alpha_i^\dagger\alpha_i, \tag{53}$$

which describes the coupling between charge (Grassmann fields) and spin [SU(2) gauge fields] degrees of freedom in the regime where double occupancy is excluded [$\mathcal{O}(J)$].

In order to account for the effect of charge and spin quantum fluctuations on the ground-state energy and magnetization of the system under hole doping and in the presence of a magnetic field, we shall consider that, in the regime of interest (stable AF phase and U values not extremely high, such that the Nagaoka phenomenon is frozen; see discussion in the end of this section), these quantum fluctuations manifest independently, i.e., the charge and spin correlation functions can be decoupled and calculated separately. Below, we show that the consistent results which come out from this procedure are highly rewarding. The above reasoning ammounts to consider that in Eq. (53), the charge correlation function is well described by the spinless tight-binding result [46,47]:

$$\sum_j\langle\alpha_i^\dagger\alpha_{i+\hat{e}_j}\rangle = \frac{1}{\pi^2}\left[\sqrt{2\pi\delta}\,\sin(\sqrt{2\pi\delta})+\frac{8}{\sqrt{3}}\sin\left(\sqrt{\frac{\pi\delta}{2}}\right)\sin\left(\sqrt{\frac{3\pi\delta}{2}}\right)\right], \tag{54}$$

where $\delta = 1 - n_\alpha$ measures the hole doping away from half-filling.

We now consider the spin sector in Eq. (53), which is described by the SU(2) gauge fields through the matrix elements: $(U_{i\alpha}^\dagger U_{i+\hat{e}_j\beta})_{\sigma,-\sigma}$ and $|(U_{i\alpha}^\dagger U_{i+\hat{e}_j\beta})_{\sigma\sigma}|^2$, in terms of the usual spin operators [38]. The latter is given in Eq. (42), whereas the former can be written as follows:

$$\left(U_{i\alpha}^\dagger U_{i+\hat{e}_j\beta}\right)_{\sigma,-\sigma} = \tfrac{1}{2}\left\{\left[1+2\left(S_{i\alpha}^z+S_{i+\hat{e}_j\beta}^z\right)+4S_{i\alpha}^zS_{i+\hat{e}_j\beta}^z\right]^{1/2}+\left[1-2\left(S_{i\alpha}^z+S_{i+\hat{e}_j\beta}^z\right)+4S_{i\alpha}^zS_{i+\hat{e}_j\beta}^z\right]^{1/2}\right\}. \tag{55}$$

At this point, it is worthwhile to introduce the vector potential, $\boldsymbol{A}$, by means of the Peierls substitution [49]: $t \longrightarrow t\exp(-i\int_{\boldsymbol{r}_i}^{\boldsymbol{r}_j}\boldsymbol{A}\cdot d\boldsymbol{r})$, which is the complex matrix element for tunneling between neighboring sites, in order to properly describes the effects of charge and spin quantum fluctuations on the ground-state properties of the AF order. Thus, inserting Eqs. (42), (54), and (55) into (53), we obtain the following effective t-J Hamiltonian:

$$\mathcal{H}^{t\text{-}J} = \frac{-2te^{-i\int_{r_i}^{r_j}\boldsymbol{A}\cdot d\boldsymbol{r}}}{z\pi^2}\left[\sqrt{2\pi\delta}\,\sin(\sqrt{2\pi\delta})+\frac{8}{\sqrt{3}}\sin\left(\sqrt{\frac{\pi\delta}{2}}\right)\sin\left(\sqrt{\frac{3\pi\delta}{2}}\right)\right]\sum_{ij\alpha\beta}\left[\sqrt{1-2S_{i+\hat{e}_j\beta}^z-2S_{i\alpha}^z+4S_{i\alpha}^zS_{i+\hat{e}_j\beta}^z}\right.$$
$$\left.+\sqrt{1+2S_{i+\hat{e}_j\beta}^z+2S_{i\alpha}^z+4S_{i\alpha}^zS_{i+\hat{e}_j\beta}^z}\right] - J(1-\delta)\sum_{ij\alpha\beta}\boldsymbol{S}_{i\alpha}\cdot\boldsymbol{S}_{i+\hat{e}_j\beta} - \frac{JNz(1-\delta)}{8} - h\sum_{i\alpha}\boldsymbol{S}_{i\alpha} + h\sum_{ij\beta}\boldsymbol{S}_{i+\hat{e}_j\beta}. \tag{56}$$

Notice that we also coupled the external homogeneous magnetic field, h, to the spins on sublattices A and B.

Let us now implement the second-order spin-wave analysis in the spin sector of Eq. (56), with the help of Eqs. (44)–(47). Further, it is convenient to choose the following Landau gauge: $\boldsymbol{A} = hx\hat{\boldsymbol{y}}$. As a result, we arrive at the following diagonalized

Hamiltonian up to $\mathcal{O}(1/S^2)$:

$$\mathcal{H}^{t\text{-}J} = \mathcal{H}_1^t + \mathcal{H}_2^J, \tag{57}$$

where the hopping Hamiltonian, $\mathcal{H}_1^t$, reads ($\boldsymbol{k}$-space)

$$\mathcal{H}_1^t = -\frac{8tze^{h\sqrt{3}/4}}{\pi^2}\left[\frac{SN}{z} + \sum_{\boldsymbol{k}}\left(\frac{1}{\sqrt{1-\gamma_{\boldsymbol{k}}^2}} - 1\right) + \frac{1}{2}\sum_{\boldsymbol{k}}\frac{\alpha_{\boldsymbol{k}}^\dagger\alpha_{\boldsymbol{k}} + \beta_{\boldsymbol{k}}^\dagger\beta_{\boldsymbol{k}}}{\sqrt{1-\gamma_{\boldsymbol{k}}^2}}\right]$$
$$\times\left[\sqrt{2\pi\delta}\,\sin(\sqrt{2\pi\delta}) + \frac{8}{\sqrt{3}}\sin\left(\sqrt{\frac{\pi\delta}{2}}\right)\sin\left(\sqrt{\frac{3\pi\delta}{2}}\right)\right], \tag{58}$$

and the exchange one, $\mathcal{H}_2^J$, becomes ($\boldsymbol{k}$-space):

$$\mathcal{H}_2^J = -\frac{zS^2J(1-\delta)N}{2} + hSN + zSJ(1-\delta)\sum_{\boldsymbol{k}}\left[\left(\sqrt{1-\gamma_{\boldsymbol{k}}^2} - 1\right) + \sqrt{1-\gamma_{\boldsymbol{k}}^2}\,(\alpha_{\boldsymbol{k}}^\dagger\alpha_{\boldsymbol{k}} + \beta_{\boldsymbol{k}}^\dagger\beta_{\boldsymbol{k}})\right]$$
$$-h\sum_{\boldsymbol{k}}\left[\left(\frac{1}{\sqrt{1-\gamma_{\boldsymbol{k}}^2}} - 1\right) + \frac{\alpha_{\boldsymbol{k}}^\dagger\alpha_{\boldsymbol{k}} + \beta_{\boldsymbol{k}}^\dagger\beta_{\boldsymbol{k}}}{\sqrt{1-\gamma_{\boldsymbol{k}}^2}}\right] - \frac{zJ(1-\delta)}{2N}\left[\sum_{\boldsymbol{k}}\left(\sqrt{1-\gamma_{\boldsymbol{k}}^2} - 1\right)\right]^2 - \frac{zJ(1-\delta)N}{8}. \tag{59}$$

Therefore the energy spectrum of $\mathcal{H}_1^t$ in the presence of a magnetic field takes the form

$$E_1 = -\frac{8tze^{h\frac{\sqrt{3}}{4}}}{\pi^2}\left[\frac{SN}{z} + \sum_{\boldsymbol{k}}\left(\frac{1}{\sqrt{1-\gamma_{\boldsymbol{k}}^2}} - 1\right)\right]\left[\sqrt{2\pi\delta}\,\sin(\sqrt{2\pi\delta}) + \frac{8}{\sqrt{3}}\sin\left(\sqrt{\frac{\pi\delta}{2}}\right)\sin\left(\sqrt{\frac{3\pi\delta}{2}}\right)\right], \tag{60}$$

whereas the one of $\mathcal{H}_2^J$ reads

$$E_2 = -\frac{zS^2J(1-\delta)N}{2} + hSN + zSJ(1-\delta)\sum_{\boldsymbol{k}}\left[\left(\sqrt{1-\gamma_{\boldsymbol{k}}^2} - 1\right)\right] - h\sum_{\boldsymbol{k}}\left[\left(\frac{1}{\sqrt{1-\gamma_{\boldsymbol{k}}^2}} - 1\right)\right]$$
$$-\frac{zJ(1-\delta)}{2N}\left[\sum_{\boldsymbol{k}}\left(\sqrt{1-\gamma_{\boldsymbol{k}}^2} - 1\right)\right]^2 - \frac{zJ(1-\delta)N}{8}. \tag{61}$$

Lastly, by adding Eqs. (60) and (61) and taking the thermodynamic limit, we find that the ground-state energy per site in the presence of a magnetic field:

$$\frac{E_h}{N} = -\frac{zS^2J(1-\delta)}{2} + hS + zSJ(1-\delta)\frac{1}{4\pi^2}\int_{\mathrm{BZ}} d^2k\left[\left(\sqrt{1-\gamma_{\boldsymbol{k}}^2} - 1\right)\right] - h\frac{1}{4\pi^2}\int_{\mathrm{BZ}} d^2k\left[\left(\frac{1}{\sqrt{1-\gamma_{\boldsymbol{k}}^2}} - 1\right)\right]$$
$$-\frac{8tze^{h\frac{\sqrt{3}}{4}}}{\pi^2}\left[\frac{S}{z} + \frac{1}{4\pi^2}\int_{\mathrm{BZ}} d^2k\left(\frac{1}{\sqrt{1-\gamma_{\boldsymbol{k}}^2}} - 1\right)\right]\left[\sqrt{2\pi\delta}\,\sin(\sqrt{2\pi\delta}) + \frac{8}{\sqrt{3}}\sin\left(\sqrt{\frac{\pi\delta}{2}}\right)\sin\left(\sqrt{\frac{3\pi\delta}{2}}\right)\right]$$
$$-\frac{zJ(1-\delta)}{32\pi^4}\left[\int_{\mathrm{BZ}} d^2k\left(\sqrt{1-\gamma_{\boldsymbol{k}}^2} - 1\right)\right]^2 - \frac{zJ(1-\delta)}{8}. \tag{62}$$

With the aim of corroborating the above analytical results with those obtained by GTPS simulations [14], let us choose $t/J = 3$, $S = 1/2$, and $z = 3$. Initially, we analyze the destruction of the AF order through the evolution of the electronic structure by increasing hole doping. Indeed, in Figs. 2(a) and 2(b), we show the evolution of the electronic structure from half-filled band ($\delta = 0$), at which the system displays a fully staggered AF order, to the doped regime at $\delta = 0.07$, which is quite close to the region of destruction of the AF phase. Moreover, after performing the integration over the first BZ zone in Eq. (62), we find that the doping-dependent ground-state energy per site at zero magnetic field can be written as follows:

$$\frac{E_0(\delta)}{NJ} = -0.3444\left[\sqrt{2\pi\delta}\,\sin(\sqrt{2\pi\delta}) + \frac{8}{\sqrt{3}}\sin\left(\sqrt{\frac{\pi\delta}{2}}\right)\sin\left(\sqrt{\frac{3\pi\delta}{2}}\right)\right] - 0.9239(1-\delta), \tag{63}$$

where one should notice that, here, for the sake of comparison with GTPS data, we have added the term $-z(1-\delta)/8$ to the exchange contribution [second term in Eq. (63)], not considered in our estimate of E_0/NJ at half-filling in Sec. V.

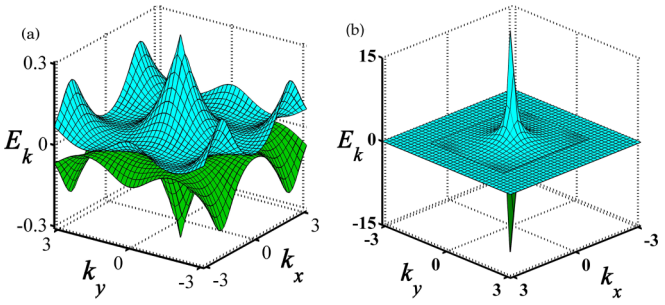

FIG. 2. (Color online) Energy spectrum of the doped AF phase at zero magnetic field and $t/J = 3$ for (a) $\delta = 0$ and (b) $\delta = 0.07$.

As shown in Fig 3(a), we compare the analytical result from Eq. (63) with the recent GTPS [14] calculations, and QMC simulations [9] at $\delta = 0$. Remarkably, our result for the doping-dependent ground-state energy agrees very well with the GTPS one up to hole doping $\delta \lesssim 0.1$. This critical value marks a region of strong magnetic instability, i.e., the breakdown of the AF order. We further indicate in the insets, Figs. 3(b) and 3(c), the effect of hole doping in the energetic contributions of the hopping and exchange Hamiltonians, respectively. Based on physics ground, one can realize that the energetic contribution due to the hopping term decreases far below zero at $\delta = 0$, as we tune up the hole doping away from half-filling, while a linear increase in the exchange energy for increasing hole doping is observed.

In order to better understand the effect of charge and spin quantum fluctuations on the AF order; we also examine the behavior of the staggered magnetization as a function of doping. In doing so, we obtain by means of Eq. (62) that the staggered magnetization per site, $m = \frac{1}{N}\frac{\partial E_h}{\partial h}|_{h=0}$, can be written as (for $S = 1/2$)

$$m(\delta) = 0.2418 - 0.1491\left[\sqrt{2\pi\delta}\,\sin(\sqrt{2\pi\delta}) + \frac{8}{\sqrt{3}}\sin\left(\sqrt{\frac{\pi\delta}{2}}\right)\sin\left(\sqrt{\frac{3\pi\delta}{2}}\right)\right]. \quad (64)$$

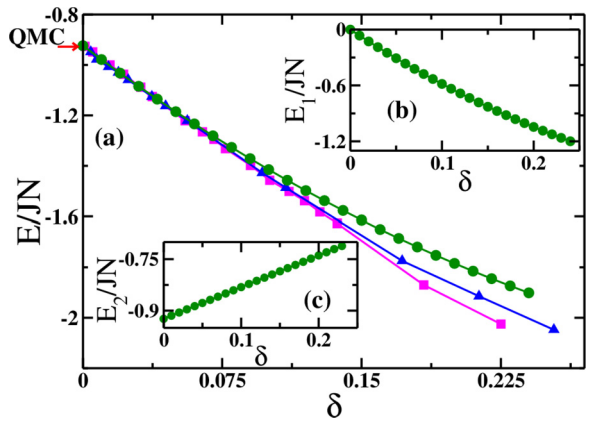

FIG. 3. (Color online) (a) Ground-state energy per site as a function of doping for $t/J = 3$. We also compare with GTPS numerical results for the virtual dimensions $D = 8$ (blue color) and $D = 12$ (magenta color). (Insets) Energetic contributions of the (b) hopping and (c) exchange terms [see Eqs. (60) and (61), or first and second term in Eq. (63), respectively].

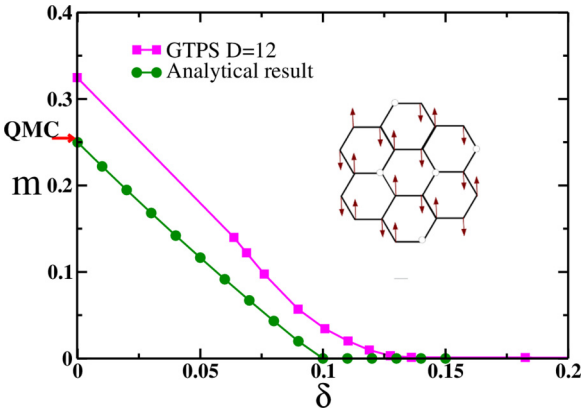

FIG. 4. (Color online) Staggered magnetization per site as a function of doping. We also benchmark against GTPS simulations for the virtual dimension $D = 12$. (Inset) Illustration of the low hole doped AF phase.

It is very important to stress the origin of the two contributions in Eq. (64): the first term stands for the Zeeman contribution to m (value of m at half-filling), while the second term is the orbital contribution to m calculated by means of the Peierls substitution. Indeed, as seen in Fig. 4, the analytical result in Eq. (64) indicates that both charge and spin quantum fluctuations conspire for the breakdown of the AF order at $\delta \approx 0.1$. As a benchmark, we also display the GTPS simulations for the virtual dimension $D = 12$ (Ref. [14]). Indeed, these findings are in good agreement for the critical hole concentration $\delta_c \approx 0.1$ beyond which the AF phase disappears. However, at half-filling ($\delta = 0$), the GTPS calculation has suggested a higher value for $m = 0.3239$ ($D = 12$), while QMC simulations [9] have found $m \approx 0.2681(8)$, closer to our value $m \approx 0.2418$. Notwithstanding, taking into account that the results for the ground-state energy and magnetization from quite distinct techniques (numerical and analytical) are compatible, we are confident that our analytical approach is indeed highly rewarding and claims for further development on this challenging topic.

We close this section by mentioning that the physical framework described by Eqs. (54) and (55) is in agreement with density-matrix renormalization-group results (DMRG) for hole-doped AB_2 t-J chains [48] with similar J values, in which case the holes exhibit charge-density order in anti-phase with the corresponding spin-density order. Accordingly, a similar behavior of m versus δ has also been observed in the low-doped regime of AB_2 t-J chains.

VII. CONCLUDING REMARKS

We reported in detail an analytical investigation of the large-U Hubbard model on the honeycomb lattice at half-filling and in the hole-doped regime. Our approach, based on field-theoretic methods, has the advantage of allowing us to derive the Lagrangian density related to the charge and spin degrees of freedom in a controllable scheme. As a result, we diagonalized exactly the Hamiltonian associated with the charge degrees of freedom only, in which case the electronic spectrum exhibits a charge Hubbard gap separating the Dirac cones. In the strong-coupling regime, by performing a perturbative expansion in

the parameter t/U up to $\mathcal{O}(J = 4t^2/U)$, we were able to derive a low-energy theory suitable to describe the quantum antiferromagnetic phase (AF) as a function of hole doping.

At half-filling (quantum Heisenberg model), we have used second-order spin-wave perturbation theory $[\mathcal{O}(1/S^2)]$ to study the effect of quantum spin fluctuations on the ground-state energy and staggered magnetization of the AF order. The results are in very good agreement with previous numerical and analytical investigations. Furthermore, in the continuum, we derived a nonlinear σ model with a topological Hopf term that describes the AF-VBS competition, although numerical studies of the Hubbard model indicate a continuous quantum phase transition from a semimetal (weak-coupling regime) to an AF phase (strong-coupling regime).

Finally, we stress that the most challenging aspect of our analysis was the mapping of the hole-doped large-U Hubbard model onto a t-J Hamiltonian; and the formulation of a controllable perturbative scheme to analyze the role played by charge and spin quantum fluctuations on the breakdown of the hole-doped AF phase. In fact, our findings for the doping-dependent ground-state energy and staggered magnetization are quite consistent with recent GTPS numerical studies.

ACKNOWLEDGMENTS

We appreciate the interesting discussions with R.R. Montenegro-Filho. This work was supported by the following Brazilian agencies: the National Council for Scientific and Technological Development (CNPq), the Fundação de Amparo à Ciência e Tecnologia do Estado de Pernambuco (FACEPE/PRONEX), and the Coordenação de Aperfeiçoamento de Pessoal de Nível Superior (CAPES).

APPENDIX: DERIVATION OF THE NONLINEAR σ MODEL WITH A TOPOLOGICAL HOPF TERM

In this Appendix, our goal is to derive the nonlinear σ model, i.e., to explicit the spin fluctuations by integrating out the fermions degrees of freedom; as well as to analyze the presence of the topological Hopf term which is crucial in describing the Néel-VBS competition [21–24]. Hence, let us turn the Lagrangian in Eq. (37) into the $\boldsymbol{\phi}$ representation, where the five-component unit vector $\boldsymbol{\phi}_{i\alpha}$ is composed by the Néel vector, $\boldsymbol{n}_{i\alpha}$, and the VBS order parameter, $\boldsymbol{\rho}_{i\alpha}$, such that $\boldsymbol{\phi}_{i\alpha} = (n^1_{i\alpha}, n^2_{i\alpha}, n^3_{i\alpha}, \rho^4_{i\alpha}, \rho^5_{i\alpha})$.

In order to write down the effective Lagrangian density in Eq. (37) in the $\boldsymbol{\phi}$ representation, we introduce the following representation of the SU(4) group [50]: $U_{i\alpha} = \cos(\lambda) - i\sin(\lambda)\boldsymbol{\phi}_{i\alpha}\cdot\boldsymbol{\Gamma}$, where λ is a group parameter and $\boldsymbol{\Gamma}$ are the usual Dirac gamma matrices. Here, we need a set of five $\boldsymbol{\Gamma}$ matrices and among the possible choices [50], we use $\Gamma_{1,2,3} = \sigma_{x,y,z}\otimes\sigma_y$, $\Gamma_4 = \sigma_0\otimes\sigma_x$, and $\Gamma_5 = \sigma_0\otimes\sigma_z$. Also, notice that these matrices satisfy the anticommuting relation $\{\Gamma_\mu,\Gamma_\nu\} = 2\delta_{\mu\nu}$ and $\Gamma_5 = -\Gamma_1\Gamma_2\Gamma_3\Gamma_4$. Hence, by using the above SU(4) representation of $U_{i\alpha}$, along with the approximation $\partial_\tau\boldsymbol{\phi}_{i\alpha}\times\boldsymbol{\phi}_{i\alpha}\approx\partial_\tau\boldsymbol{\phi}_{i\alpha}$, we find that the effective Lagrangian density, $\mathcal{L}$, in Eq. (37) assumes the form

$$\mathcal{L} \approx \sum_i \alpha_i^\dagger\partial_\tau\alpha_i + \frac{J}{8t}\sum_{ij\alpha}(1 + i\boldsymbol{\phi}_{i\alpha}\cdot\boldsymbol{\Gamma})[\alpha_i^\dagger(\alpha_{i+e_j} + \alpha_{i-e_j}) + \text{H.c.}]. \tag{A1}$$

We would like to mention that terms which depend on the total time derivative and irrelevant additive constant were excluded (such terms do not contribute to the effective action).

In the sequence, we take the continuum limit in Eq. (A1), such that the partition function takes the form

$$Z \approx \int D\bar{\alpha}D\alpha e^{-S_{\text{eff}}} = \int D\bar{\alpha}D\alpha\exp\left\{\int d^3x\bar{\alpha}[i\tau_\mu\partial_\mu + ig\tilde{\phi}_{i\alpha}]\alpha\right\}, \tag{A2}$$

where $\boldsymbol{\tau}$ are the Pauli matrices; besides, we have defined $\bar{\alpha}\equiv i\tau_z\alpha^\dagger$, $g\equiv J/4t$, and $\tilde{\phi}_{i\alpha}\equiv\boldsymbol{\phi}\cdot\boldsymbol{\Gamma}$. Correspondingly, by means of the standard procedures [39,40], we can write down the effective action as

$$S_{\text{eff}} = \ln\det(i\tau_\mu\partial_\mu + ig\tilde{\phi}_{i\alpha}). \tag{A3}$$

At this stage, we follow Abanov and Wiegmann [51,52], and write the Dirac operator in the form $\mathcal{D} = i\tau_\mu\partial_\mu + ig\tilde{\phi}_{i\alpha}$, which allow us to rewrite the fermionic determinant in Eq. (A3) in a suitable form to evaluate a perturbative expansion. Hence, by calculating the variation of the effective action, S_{eff}, with respect to $\boldsymbol{\phi}$, we get

$$\delta S_{\text{eff}} = -\text{Tr}\left(\frac{\delta D D^\dagger}{-\partial^2 + g^2 - g\tau_\mu\partial_\mu\tilde{\phi}}\right). \tag{A4}$$

Now, by applying the perturbative expansion up to first order in $g\tau_\mu\partial_\mu\tilde{\phi}$, we find that the real contribution of Eq. (A4) yields the nonlinear σ model [51–53]:

$$S_{\text{Re}} = \frac{g}{4\pi}\int d^3x(\partial_\mu\boldsymbol{\phi})^2. \tag{A5}$$

Also, there exist an imaginary contribution which gives rise to the topological Hopf term. With the purpose of making its derivation explicit, we must add a parameter ξ such that the field $\tilde{\phi}_{i\alpha}(x,\xi)$ continuously interpolates between the constant value $\tilde{\phi}_{i\alpha}(x,\xi=0) = (0,0,0,0,1)$ and the physical value $\tilde{\phi}_{i\alpha}(x,\xi=1) = \tilde{\phi}_{i\alpha}(x)$. This leads to

$$S_{\text{Im}} = -i\frac{\epsilon_{abcde}}{12\pi}\int_0^1 d\xi\int d^3x\phi^a\partial_\tau\phi^b\partial_x\phi^c\partial_y\phi^d\partial_\xi\phi^e. \tag{A6}$$

It is also worthwhile to introduce, without loss of generality, the four-component unit vector $\boldsymbol{\pi}$ according to the following parametrization: $\phi^a = \sin(\xi\varphi)\pi^a$, $\phi^b = \sin(\xi\varphi)\pi^b$, $\phi^c = \sin(\xi\varphi)\pi^c$, $\phi^d = \sin(\xi\varphi)\pi^d$ and $\phi^e = \cos(\xi\varphi)$. Thus, integrating over the auxiliary variable ξ, we find that

$$S_{\text{Im}} = -i\frac{\epsilon^{\mu\nu\lambda}\epsilon_{abcd}}{12\pi}\int d^3x\left[1 - \frac{9}{8}\cos(\varphi) + \frac{1}{8}\cos(3\varphi)\right] \times\pi^a\partial_\mu\pi^b\partial_\nu\pi^c\partial_\lambda\pi^d, \tag{A7}$$

where we can readily identify the topological Hopf term [23,51–53]

$$H = \frac{\epsilon_{abcd}}{12\pi^2}\int d^3x\pi^a\partial_\tau\pi^b\partial_x\pi^c\partial_y\pi^d \tag{A8}$$

and the θ term

$$\theta = \pi\left[1 - \frac{9}{8}\cos(\varphi) + \frac{1}{8}\cos(3\varphi)\right]. \tag{A9}$$

Lastly, by summing up Eqs. (A5) and (A7), we obtain the action of the nonlinear σ model with a Hopf term:

$$S = \frac{g \sin^2 \varphi}{4\pi} \int d^3x (\partial_\mu \boldsymbol{\pi})^2 - i\theta H. \tag{A10}$$

We would like to mention that by introducing a CP^{n-1} formulation this action can be mapped onto a bosonic representation with the well-known Chern-Simons term [23,39,51].

This nonlinear σ model with the extra topological term describes the AF-VBS competition [21–24]. It is expected that, as the Coulombian interaction U varies, which means to tune the coupling constant g, so that the two insulating phases become accessible in distinct regimes (quite possibly in generalized Heisenberg models). The key point in the analysis of these two distinct ground states is to make explicit the hedgehog topological defect in the Néel order parameter. In order to realize this monopole configuration we parametrize the components of the four-component unit $\boldsymbol{\pi}$ in terms of the Néel vector as follows: $\pi^a = \sin(\upsilon) n^a$; $\pi^b = \sin(\upsilon) n^b$; $\pi^c = \sin(\upsilon) n^c$ and $\pi^d = \cos(\upsilon)$, such that we can write down the Lagrangian density, $\mathcal{L}_{\rm BP}$, associated with the Berry phase term in Eq. (A7) as

$$\mathcal{L}_{\rm BP} = \frac{i}{3}(2\upsilon - \sin 2\upsilon)\left[1 - \frac{9}{8}\cos(\varphi) + \frac{1}{8}\cos(3\varphi)\right]\rho_m, \tag{A11}$$

where

$$\rho_m = \frac{\epsilon_{abc}}{4\pi} \partial_\tau (n^a \partial_x n^b \partial_y n^c) \tag{A12}$$

is the monopole charge density. Thus when the monopole charge density ρ_m is integrated over the space-time configuration of $\boldsymbol{n}$ there exists a change in the Skyrmion number: $\Delta Q_{xy} = \int d\tau dx dy \rho_m$.

These monopoles proliferate at the deconfined AF-VBS critical point. Indeed, it has been shown that the presence of such monopole events correctly describes the quantum paramagnet VBS order [53–55], which spontaneously breaks lattice (e.g., translational) symmetry. We may also identify the Berry phase, which leads to the VBS order by setting $\varphi = \pi/2$ together with the following set of $\upsilon = \{0, \pi, 2\pi\}$ in Eq. (A11), in which case we find $S_{\rm BP} = 1$, $e^{2i\pi/3\Delta Q_{xy}}$, and $e^{4i\pi/3\Delta Q_{xy}}$, respectively, which correspond to a Berry phase shift equal to $2i\pi/3\Delta Q_{xy}$ [55]; in fact, by applying the symmetry operation in the honeycomb lattice we can construct the VBS order with distinct patterns [23].

[1] A. H. Castro Neto, F. Guinea, N. M. R. Peres, K. S. Novoselov, and A. K. Geim, The electronic properties of graphene, Rev. Mod. Phys. **81**, 109 (2009); V. N. Kotov, B. Uchoa, V. M. Pereira, F. Guinea, and A. H. Castro Neto, Electron-electron interactions in graphene: Current status and perspectives, *ibid.* **84**, 1067 (2012).

[2] V. Kataev, A. Möller, U. Löw, W. Jung, N. Schittner, M. Kriener, and A. Freimuth, Structural and magnetic properties of the new low-dimensional spin magnet $InCu_{2/3}V_{1/3}O_3$, J. Magn. Magn. Mater. **290-291**, 310 (2005).

[3] A. Möller, U. Löw, T. Taetz, M. Kriener, G. André, F. Damay, O. Heyer, M. Braden, and J. A. Mydosh, Structural domain and finite-size effects of the antiferromagnetic $S = 1/2$ honeycomb lattice in $InCu_{2/3}V_{1/3}O_3$, Phys. Rev. B **78**, 024420 (2008).

[4] Y. J. Yan, Z. Y. Li, T. Zhang, X. G. Luo, G. J. Ye, Z. J. Xiang, P. Cheng, L. J. Zou, and X. H. Chen, Magnetic properties of the doped spin-1/2 honeycomb-lattice compound $In_3Cu_2VO_9$, Phys. Rev. B **85**, 085102 (2012).

[5] Y. Miura, R. Hirai, Y. Kobayashi, and M. Sato, Spin-gap behavior of $Na_3Cu_2SbO_6$ with distorted honeycomb structure, J. Phys. Soc. Jpn. **75**, 084707 (2006).

[6] S. A. J. Kimber, I. I. Mazin, J. S. Shen, H. O. Jeschke, S. V. Streltsov, D. N. Argyriou, R. Valentí, and D. I. Khomskii, Valence bond liquid phase in the honeycomb lattice material Li_2RuO_3, Phys. Rev. B **89**, 081408(R) (2014).

[7] Y. Singh and P. Gegenwart, Antiferromagnetic Mott insulating state in single crystals of the honeycomb lattice material Na_2IrO_3, Phys. Rev. B **82**, 064412 (2010).

[8] J. D. Reger, J. A. Riera, and A. P. Young, Monte Carlo simulations of the spin-1/2 Heisenberg antiferromagnet in two dimensions, J. Phys. Condens. Matter **1**, 1855 (1989).

[9] U. Löw, Properties of the two-dimensional spin-1/2 Heisenberg model on a honeycomb lattice with interlayer coupling, Condens. Matter Phys. **12**, 497 (2009).

[10] Z. Weihong, J. Oitmaa, and C. J. Hamer, Second-order spin-wave results for the quantum XXZ and XY models with anisotropy, Phys. Rev. B **44**, 11869 (1991).

[11] J. Oitmaa, C. J. Hamer, and Z. Weihong, Quantum magnets on the honeycomb and triangular lattices at $T = 0$, Phys. Rev. B **45**, 9834 (1992).

[12] H. C. Jiang, Z. Y. Weng, and T. Xiang, Accurate determination of tensor network state of quantum lattice models in two dimensions, Phys. Rev. Lett. **101**, 090603 (2008); Z. Y. Xie, H. C. Jiang, Q. N. Chen, Z. Y. Weng, and T. Xiang, Second renormalization of tensor network states, *ibid.* **103**, 160601 (2009).

[13] H. H. Zhao, Z. Y. Xie, Q. N. Chen, Z. C. Wei, J. W. Cai, and T. Xiang, Renormalization of tensor-network states, Phys. Rev. B **81**, 174411 (2010).

[14] Z.-C. Gu, H.-C. Jiang, D. N. Sheng, H. Yao, L. Balents, and X. G. Wen, Time-reversal symmetry breaking superconducting ground state in the doped Mott insulator on the honeycomb lattice, Phys. Rev. B **88**, 155112 (2013).

[15] Z. Y. Meng, T. C. Lang, S. Wessel, F. F. Assaad, and A. Muramatsu, Quantum spin liquid emerging in two-dimensional correlated Dirac fermions, Nature (London) **464**, 847 (2010).

[16] H. T. Diep, *Frustrated Spin Systems* (World Scientific, New Jersey, 2004); 2nd ed. (World Scientific, New Jersey, 2013).

[17] H. Mosadeq, F. Shahbazi, and S. A. Jafari, Plaquette valence bond ordering in a J_1-J_2 Heisenberg antiferromagnet on a honeycomb lattice, J. Phys. Condens. Matter **23**, 226006 (2011).

[18] A. F. Albuquerque, D. Schwandt, B. Hetényi, S. Capponi, M. Mambrini, and A. M. Läuchli, Phase diagram of a frustrated quantum antiferromagnet on the honeycomb lattice: Magnetic order versus valence-bond crystal formation, Phys. Rev. B **84**, 024406 (2011).

[19] R. Ganesh, J. van den Brink, and S. Nishimoto, Deconfined criticality in the frustrated Heisenberg honeycomb antiferromagnet, Phys. Rev. Lett. **110**, 127203 (2013).

[20] Z. Zhu, D. A. Huse, and S. R. White, Weak plaquette valence bond order in the $S = 1/2$ honeycomb J_1-J_2 Heisenberg model, Phys. Rev. Lett. **110**, 127205 (2013).

[21] O. I. Motrunich and A. Vishwanath, Emergent photons and transitions in the O(3) sigma model with hedgehog suppression, Phys. Rev. B **70**, 075104 (2004).

[22] T. Senthil, A. Vishwanath, L. Balents, S. Sachdev, and M. P. A. Fisher, Deconfined quantum critical points, Science **303**, 1490 (2004); T. Senthil, L. Balents, S. Sachdev, A. Vishwanath, and M. P. A. Fisher, Quantum criticality beyond the Landau-Ginzburg-Wilson paradigm, Phys. Rev. B **70**, 144407 (2004).

[23] L. Fu, S. Sachdev, and C. Xu, Geometric phases and competing orders in two dimensions, Phys. Rev. B **83**, 165123 (2011).

[24] C. Xu, Unconventional quantum critical points, Int. J. Mod. Phys. B **26**, 1230007 (2012), and references therein.

[25] S. Sorella, Y. Otsuka, and S. Yunoki, Absence of a spin liquid phase in the Hubbard model on the honeycomb lattice, Sci. Rep. **2**, 992 (2012); see, also, T. Paiva, R. T. Scalettar, W. Zheng, R. R. P. Singh, and J. Oitmaa, Ground-state and finite-temperature signatures of quantum phase transitions in the half-filled Hubbard model on a honeycomb lattice, Phys. Rev. B **72**, 085123 (2005).

[26] Y. Izyumov, Strongly correlated electrons: the t-J model, Phys. Usp. **40**, 445 (1997).

[27] P. A. Lee, N. Nagaosa, and X. G. Wen, Doping a Mott insulator: physics of high-temperature superconductivity, Rev. Mod. Phys. **78**, 17 (2006).

[28] M. Ogata and H. Fukuyama, The t-J model for the oxide high-T_c superconductors, Rep. Prog. Phys. **71**, 036501 (2008).

[29] N. M. R. Peres, M. A. N. Araújo, and D. Bozi, Phase diagram and magnetic collective excitations of the Hubbard model for graphene sheets and layers, Phys. Rev. B **70**, 195122 (2004); M. A. N. Araújo and N. M. R. Peres, Weak ferromagnetism and spiral spin structures in honeycomb Hubbard planes, J. Phys. Condens. Matter **18**, 1769 (2006).

[30] G.-Y. Sun and S.-P. Kou, Possible anomalous spin dynamics of the Hubbard model on a honeycomb lattice, J. Phys. Condens. Matter **23**, 045603 (2011).

[31] R. L. Stratonovich, On a method of calculating quantum distribution functions, Dokl. Akad. Nauk SSSR **115**, 1094 (1957) [Sov. Phys. Dokl. **2**, 416 (1958)]; J. Hubbard, Calculation of partition functions, Phys. Rev. Lett. **3**, 77 (1959).

[32] C. A. Macêdo, M. D. Coutinho-Filho, and M. A. de Moura, Critical study of the functional-integral method applied to the itinerant magnetism, Phys. Rev. B **25**, 5965 (1982); C. A. Macêdo and M. D. Coutinho-Filho, Hubbard model: functional-integral approach and diagrammatic perturbation theory, *ibid.* **43**, 13515 (1991).

[33] M. L. Lyra, M. D. Coutinho-Filho, and A. M. Nemirovsky, Hubbard model: Field theory and critical phenomena, Phys. Rev. B **48**, 3755 (1993).

[34] H. J. Schulz, Effective action for strongly correlated fermions from functional integrals, Phys. Rev. Lett. **65**, 2462 (1990).

[35] Z. Y. Weng, C. S. Ting, and T. K. Lee, Path-integral approach to the Hubbard model, Phys. Rev. B. **43**, 3790(R) (1991).

[36] Z. Y. Weng, Dynamical spiral state at finite doping, Phys. Rev. Lett. **66**, 2156 (1991).

[37] Z. Y. Weng, D. N. Sheng, C. S. Ting, and Z. B. Su, One-dimensional large-U Hubbard model: An analytical approach, Phys. Rev. Lett. **67**, 3318 (1991); Path-integral approach to the one-dimensional large-U Hubbard model, Phys. Rev. B **45**, 7850 (1992).

[38] M. H. Oliveira, E. P. Raposo, and M. D. Coutinho-Filho, AB_2 Hubbard chains in the strong-coupling limit: Ferrimagnetism, Nagaoka and RVB states, phase separation, and Luttinger-liquid behavior, Phys. Rev. B **80**, 205119 (2009).

[39] E. Fradkin, *Field Theories of Condensed Matter Systems* (Cambrigde University Press, Cambrigde, 2013).

[40] H. Kleinert *Path Integral in Quantum Mechanics, Statistics and Polymer Physics* (World Scientific, New Jersey, 1995).

[41] X. G. Wen, *Quantum Field Theory of Many-Body Systems* (Oxford University Press, Oxford, 2010).

[42] W. K. Tung, *Group Theory in Physics* (World Scientific, New Jersey, 2010).

[43] A. Giuliani and V. Mastropietro, The two-dimensional Hubbard model on the honeycomb lattice, Commun. Math. Phys. **293**, 301 (2010).

[44] A. M. S. Macêdo, M. C. dos Santos, M. D. Coutinho-Filho, and C. A. Macêdo, Magnetism and phase separation in polymeric Hubbard chains, Phys. Rev. Lett. **74**, 1851 (1995).

[45] A. Auerbach, *Interacting Eletrons and Quantum Magnetism* (Springer-Verlag, New York, 1994).

[46] R. R. Montenegro-Filho and M. D. Coutinho-Filho, Doped AB_2 Hubbard chain: Spiral, Nagaoka and resonating-valence-bond states, phase separation, and Luttingerliquid behavior, Phys. Rev. B **74**, 125117 (2006).

[47] C. Vitoriano and M. D. Coutinho-Filho, Fractional statistics and quantum scaling properties of the integrable Penson-Kolb-Hubbard chain, Phys. Rev. B **82**, 125126 (2010).

[48] R. R. Montenegro-Filho and M. D. Coutinho-Filho, Magnetic and nonmagnetic phases in doped AB_2 t-J Hubbard chains, Phys. Rev. B **90**, 115123 (2014).

[49] F. H. L. Essler, H. Frahm, F. Göhmann, A. Klümper, and V. E. Korepin, *The One-Dimensional Hubbard Model* (Cambrigde University Press, Cambrigde, 2010).

[50] V. M. Red'kov, A. A. Bogush, and N. G. Tokarevskaya, On parametrization of the linear GL(4,C) and unitary SU(4) groups in terms of Dirac matrices, Sigma **4**, 021 (2008).

[51] A. G. Abanov, Hopf term induced by fermions, Phys. Lett. B **492**, 321 (2000).

[52] A. G. Abanov and P. B. Wiegmann, Theta-terms in nonlinear sigma-models, Nucl. Phys. B **570**, 685 (2000).

[53] A. Tanaka and X. Hu, Many-body spin Berry phases emerging from the π-flux state: Competition between antiferromagnetism and the valence-bond-solid state, Phys. Rev. Lett. **95**, 036402 (2005).

[54] F. D. M. Haldane, O(3) nonlinear σ model and the topological distinction between integer- and half-integer-spin antiferromagnets in two dimensions, Phys. Rev. Lett. **61**, 1029 (1988).

[55] N. Read and S. Sachdev, Valence-bond and spin-Peierls ground states of low-dimensional quantum antiferromagnets, Phys. Rev. Lett. **62**, 1694 (1989); Spin-Peierls, valence-bond solid, and Néel ground states of low-dimensional quantum antiferromagnets, Phys. Rev. B **42**, 4568 (1990).